Enhanced Energy Conversion Efficiency of Mg2+−Modified Mesoporous TiO2 Nanoparticles Electrodes for Dye−Sensitized Solar Cells

ARTICLE *in* THE JOURNAL OF PHYSICAL CHEMISTRY C · NOVEMBER 2010

Impact Factor: 4.77 · DOI: 10.1021/jp108446n

4 AUTHORS, INCLUDING:

Tianyou Peng
Wuhan University
214 PUBLICATIONS **5,217** CITATIONS
SEE PROFILE

Ke Fan
KTH Royal Institute of Technology
34 PUBLICATIONS **573** CITATIONS
SEE PROFILE

Enhanced Energy Conversion Efficiency of Mg^{2+}-Modified Mesoporous TiO_2 Nanoparticles Electrodes for Dye-Sensitized Solar Cells

Tianyou Peng,*,†,‡ Ke Fan,† De Zhao,† and Junnian Chen†

College of Chemistry and Molecular Science, Wuhan University, Wuhan 430072, People's Republic of China, and State Key Laboratory of Rare Earth Materials Chemistry and Applications, Peking University, Beijing 100871, China

Received: September 4, 2010; Revised Manuscript Received: October 30, 2010

Mesoporous TiO_2 (m-TiO_2) nanoparticles were used to prepare the porous electrodes for dye-sensitized solar cells (DSSCs). Experimental results indicate that the MgO covered on TiO_2 electrode can act as barrier layer for the interfacial charge recombination processes, whereas some MgO immingled among TiO_2 networks due to the part reconstruction of the electrode during the second annealing process can retard the electron transport within electrode. The optimal conversion efficiency is obtained from solar cell fabricated with TiO_2 electrode modified with 0.2 M Mg^{2+} solution, with a 39% improvement in the efficiency as compared to the unmodified one. The suppression of interfacial charge recombination and the enhanced dye adsorption capacity contribute to the improved photovoltaic performance for the Mg^{2+}-modified electrode, and the retardation of electron transport and injection by excessive Mg^{2+} modification is responsible for the efficiency losses of the corresponding TiO_2-based solar cell. This indicates that controlling the extrinsic parameters such as the electron transport and recombination is very important to improve the photovoltaic performance of TiO_2-based solar cell.

1. Introduction

Dye-sensitized solar cells (DSSCs) are of great interest as an alternative to the conventional Si-based device because of their low-cost production and high performance.[1,2] After more than one decade's development, the overall energy conversion efficiency has already enhanced to more than 10% under AM1.5 simulated sunlight.[1−4] Generally, the high efficiency achieved with DSSCs may be attributed to the larger surface area of porous TiO_2 electrode, more efficient visible light absorption of dye molecules, and the interfacial electron transfer among the film/electrolyte/counter electrode interfaces.[1,2] However, an unusual feature of these porous film-based solar cells is the lack of depletion layer at the electrode/dye/electrolyte interfaces;[1−4] therefore, the back electron transfer (i.e., charge recombination) that occurred at the interfaces still remains one of the major limiting factors for enhancing the cell performance.[3−9]

The suppression of charge recombination, as demonstrated by high open-circuit photovoltage (V_{oc}), was achieved by passivating the recombination centers at the TiO_2 film with the addition of 4-*tert*-butylpyridine to the electrolyte.[3] Moreover, the efficiency of solar cell was also improved by surface modification due to the formed barrier layer, which can reduce the dark current contributed by the interfacial charge recombination.[4−9] Up until now, the reported surface modification materials for TiO_2 electrode included large bandgap semiconducting oxides, such as ZnO,[4] Nb_2O_5,[5] and WO_3,[6] and electronic-insulating materials, such as SrO,[7] Al_2O_3,[8,9] ZrO_2, and SiO_2.[9] The improved efficiency of solar cell has been attributed to the following two factors: First, the wide bandgap overlayer as a barrier layer retards the back electron transfer at the electrode/dye/electrolyte interfaces and minimizes the charge recombination.[4−8] Second, the overlayer enhances the dye adsorption, leading to the improved cell performance.[9−11] If the coating oxide is more basic than TiO_2, the carboxyl groups in dye molecule are more easily adsorbed to the surfaces of overlayer.[9−11] For example, Palomares and co-workers[9] addressed the ability of metal oxide (SiO_2, Al_2O_3, and ZrO_2) insulating overlayer on TiO_2 electrode to retard the interfacial recombination and found that the most basic overlayer, Al_2O_3 with point of zero charge (PZC) of 9.2, is optimal for retarding the interfacial recombination, and the solar cell fabricated with TiO_2 Al_2O_3-coated electrode led to an increase in V_{oc} up to 50 mV and a 35% improvement in efficiency. The performance for the TiO_2 electrodes depends on the differences in acid/base properties of the overlayer.[9−11]

As insulating oxide, MgO with bandgap (6.0−7.8 eV) much wider than TiO_2 (3.0−3.2 eV), has also been employed to improve the efficiency of TiO_2-based solar cell.[10−14] For example, Jung et al.[10] found the efficiency of MgO-coated TiO_2 increased by 45% as compared to the pure TiO_2. Kumara et al.[12] and Taguchi et al.[13] also reported that an MgO shell on TiO_2 can retard the recombination of holes and back-transferred electrons, and then improve the cell efficiency. In addition to the retarded charge recombination, however, MgO coating has another potential advantage to improve the cell efficiency. As compared to the acidic TiO_2 with PZC of 6.5, as coating layer, MgO with PZC of 12.0, which is supposed to be the highest basic oxide, is more beneficial for the dye molecule adsorbed to the electrode surfaces.[10,11] The above investigations remind us that MgO surface modification is probably a potential way to improve the efficiency of TiO_2-based DSSCs.[10−14]

TiO_2 nanoparticles with intraparticle mesostructures (m-TiO_2) have been fabricated and show much better photoactivity than do the commercially available nonporous TiO_2 nanoparticles (Degussa P25, Germany) due to its high specific surface area and well-crystallized mesoporous wall within the nanoparticles

* To whom correspondence should be addressed. Phone: 86-27-6875-2237. Fax: 86-27-6875-2237. E-mail: typeng@whu.edu.cn.
† Wuhan University.
‡ Peking University.

10.1021/jp108446n
Published on Web 11/29/2010

as reported in our previous publications.[15,16] Recently, these m-TiO_2 nanoparticles were applied to prepare the porous electrode for DSSCs, which show much better conversion efficiency than the P25-based solar cell.[17] The electrical impedance spectroscopy (EIS) and the open-circuit voltage decay curve (OCVD) measurements were applied to examine the interfacial recombination kinetic processes involved in the operation of DSSCs.[2,17−21] It was found that the intraparticle pores within m-TiO_2 nanoparticles cannot be covered by dye molecules during the film coloring and then become the situation of dark reaction.[2,17] It is rational to consider that the surface modification might overcome this drawback of m-TiO_2 electrode by preventing the dark reaction and further improve the performance of above m-TiO_2-based cell.[8−10] However, the coating processes mentioned above, which usually apply sol derived from their respective alkoxide,[8−10] are not suitable for the present m-TiO_2 film due to the high viscosity of sol and small intraparticle pores within m-TiO_2 nanoparticles. Herein, we address in detail the surface modifications of m-TiO_2 film with $Mg(NO_3)_2$ solution through dipping and annealing processes,[7] focusing on the effects of the Mg^{2+} concentration on the surface states and charge recombination of TiO_2 electrode, and thereby improving the efficiency of solar cell fabricated with m-TiO_2 electrode. The highest efficiency was obtained for the m-TiO_2 electrode modified with 0.2 M Mg^{2+} solution, with a 39% improvement in the efficiency as compared to the unmodified one.

2. Experimental Section

2.1. Materials Preparation. ***m-TiO_2 Nanoparticles Preparation.*** TiO_2 nanoparticles with intraparticle mesostructures (m-TiO_2) were prepared via a surfactant templating process.[15] The as-prepared samples were dried at 80 °C, and then calcined at 300 °C with a heating rate of 2 °C min^{-1} for 7 h. The microstructures and physical properties of m-TiO_2 nanoparticles were reported in our previous publications.[15,16] N719 dye, $Ru(dcbpy)_2(NCS)_2$ (*cis*-bis(2,2′-bipyridyl-4,4′- dicarboxylato)-ruthenium(II)-bis-tetrabutylammonium), was purchased from Solaronix S. A.

Photoelectrode Preparation. Doctor-blade technique was adopted to prepare the porous electrode on a conducting glass (FTO, F-doped SnO_2, 15−20 Ω $sq.^{-1}$),[17] which has been rinsed with distilled water and immersed in isopropanol for 2 h to increase its hydrophilicity.

1.0 g of m-TiO_2, 4.3 mL of dry alcohol, 1.4 mL of HCl solution (0.1 M), and 0.3 mL of acetylacetone were mixed in a PTFE container, and then dispersed through ball-milling. The resulting paste was dropped and spread uniformly onto the conducting glass (4 cm × 4 cm) with adhesive tape serving as spacers. The film was dried under ambient condition and annealed at 500 °C for 1 h, and then incised into smaller pieces to obtain TiO_2 film with the same thickness (ca. 4.45 μm). The Mg^{2+}-modified TiO_2 electrode was fabricated by dipping the m-TiO_2 electrode in $Mg(NO_3)_2$ solution for 60 min, and annealed at 500 °C for 1 h. The obtained films are denoted as 0.*x* Mg−TiO_2, in which 0.*x* represents the Mg^{2+} concentration used. To keep similar conditions between the standard and modified electrodes, the m-TiO_2 electrodes without modifications were annealed at the same times as the modified ones. Dye-sensitization was achieved by immersing the electrode in a 0.3 mM dye ethanol solution overnight, followed by rinsing in ethanol and drying.

DSSCs Fabrication. The dye-sensitized electrode was assembled in a typical sandwich-type cell; the identical platinized FTO counter-electrode was placed over the dye-sensitized electrode, and the electrolyte, containing 0.5 M LiI, 0.05 M I_2, and 0.1 M 4-*tert*-butylpyridine in 1:1 acetonitrile−propylene carbonate, was sandwiched between the photoanode and the platinized counter-electrode by firm press. An adhesive tape (approximately 50 μm) was placed between the photoanode and the counter-electrode to avoid short-circuiting.

2.2. Characterization. Structure phase analyses with X-ray diffraction (XRD) method were performed on a D_8-advance X-ray diffractometer (Bruker) with Cu Kα radiation (λ = 0.15418 nm). The film thicknesses were measured with a TalyForm S4C-3D profilometer (U.K.). To estimate the adsorption capacity of dye, the dye-sensitized electrode was separately immersed into a 0.1 M NaOH solution in a mixed solvent (water/ethanol = 1:1), which resulted in desorption of N719 from the porous electrode. The absorbance of the resulted solution was measured by a UV-240 UV−vis spectrophotometer. The dye adsorptive capacity was determined by the molar extinction coefficient of 1.41×10^4 dm^3 mol^{-1} cm^{-1} at 515 nm as reported previously.[2]

2.3. Photoelectrochemical Measurements. ***Electrochemical Impedance Spectroscopy and Open-Circuit Voltage Decay Curve.*** The electrochemical impedance spectroscopy (EIS) measurements were carried out by applying bias of the open-circuit voltage (V_{oc}) without electric current and were recorded over a frequency range of 10^{-2}−10^5 Hz with ac amplitude of 10 mV. The cell was first illuminated to a steady voltage, and then the open-circuit voltage decay curve (OCVD) was recorded once the illumination was turned off by a shutter. The above measurements were carried out on a CHI-604C electrochemical analyzer (CH Instruments) combined with Xe-lamp as light source.

DSSCs Properties Test. The DSSC was illuminated by light with energy of 100 mW cm^{-2} from a 500 W Xe-lamp. The light intensity was determined using a SRC-1000-TC-QZ-N reference monocrystalline silicon cell system (Oriel, U.S.), which was calibrated by National Renewable Energy Laboratory, A2LA accreditation certificate 2236.01. Two cutoff filters were used to obtain the wavelengths in the range of 420−950 nm and prevent the generation of electron−hole pairs through direct TiO_2 bandgap excitation. Computer-controlled Keithley 2400 source meter was employed to collect the current−voltage (I−V) curves of DSSCs. The active area was 5 × 5 mm^2. The power conversion efficiency was calculated according to eq 1:

$$\eta\,(\%) = \frac{V_{oc} I_{sc} \mathrm{FF}}{P_{in}} \times 100 \qquad (1)$$

where η is the overall energy conversion efficiency, and V_{oc}, I_{sc}, and FF are the open-circuit photovoltage, the short-circuit photocurrent density, and the fill factor, respectively. P_{in} is the energy of the incident light.

3. Results and Discussion

3.1. X-ray Diffraction Analyses. Figure 1 depicts the XRD patterns of m-TiO_2 electrode and its Mg^{2+}-modified products. As can be seen, the crystal phase of m-TiO_2 film annealed at 500 °C is anatase (JCPDS, no. 21-1272). The transparent conducting oxide (FTO) layer has an obvious influence on the diffraction pattern of anatase TiO_2. One of FTO diffraction peaks overlaps with the (004) diffraction peak of anatase, and the strongest FTO peak appears as a shoulder next to the (101) diffraction peak of anatase. This phenomenon may be attributed

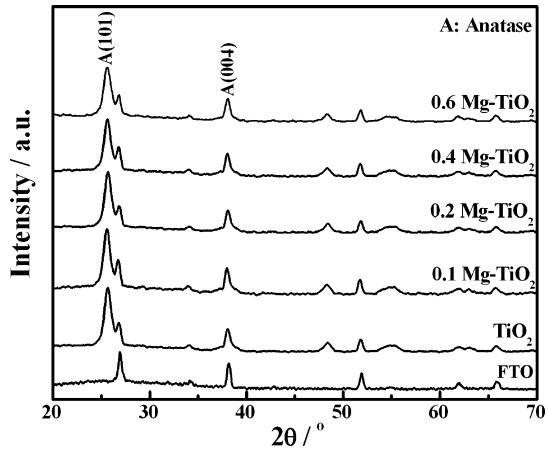

Figure 1. XRD patterns of porous m-TiO_2 electrode and its modified products derived from different Mg^{2+} concentrations.

TABLE 1: Effects of Mg^{2+}-Modification on Average Grain Size and Electron Transport/Recombination Parameters in m-TiO_2 Electrodes

electrodes	TiO_2	0.1 Mg−TiO_2	0.2 Mg−TiO_2	0.4 Mg−TiO_2	0.6 Mg−TiO_2
R_s (Ω)	15.28	15.88	17.14	16.53	15.95
R_{ct} (Ω)	17.70	16.11	14.59	15.16	14.34
R_w (Ω)	2.64	2.37	2.36	3.12	11.35
τ_n (ms)	16.30	19.72	16.30	13.36	9.13
D_{eff} ($\times 10^{-5}$ cm^2 s^{-1})	8.15	6.83	7.51	7.20	2.74
L_n (μm)	11.53	11.61	11.06	9.81	5.01
D101 (nm)	11.2	9.6	8.8	8.8	8.2

to the lesser film thickness (~4.45 μm). Moreover, there is not any diffraction peak attributable to the corresponding MgO, even for the TiO_2 film modified with 0.6 M Mg^{2+} solution, indicating that MgO may be highly dispersed/covered on the TiO_2 electrode surfaces.

According to Scherrer's formula, the average grain sizes (D101) of TiO_2 calculated from the broadening of (101) diffraction peaks are listed in Table 1. As can be seen from Figure 1, Mg^{2+}-modified TiO_2 electrode shows broader diffraction peaks than does the unmodified one, indicating the grain growth was retarded. It can be confirmed by the average grain size decreasing from 11.2 to 8.2 nm upon enhancing the Mg^{2+} concentration. It is reasonable to speculate that the nitrate or hydroxide adsorbed on electrodes can be decomposed to form MgO covered on TiO_2 film surfaces during the second annealing process at 500 °C, which is similar to the coating processes by sol process.[8−10] However, the present nitrate solution is easier to penetrate into the porous film due to its higher permeability and lower viscosity as compared to the "sol". The porous structures of m-TiO_2 film and nanoparticles could partly collapse and reconstruct, and this part collapse and reconstruction would result in some MgO remaining among TiO_2 nanoparticles of the inorgain networks during the second annealing process.[15−17] These MgO immingled in the inorganic network can retard the grain growth of TiO_2. The above different existing states of MgO would affect the crystallinity, grain size, and microstructure of the electrode, and consequently its surface and electronic properties,[1−4] which will be further discussed in the following sections.

3.2. Electrochemical Impedance Spectra of Mg^{2+}-Modified Electrode. Figure 2 shows the Nyquist (a) and Bode phase (b) plots of EIS spectra for various solar cells. The inset is the simplified model of equivalent electric circuit for the operating state of DSSC.[2,20−22] Among those, R_{FTO} is the resistance of conductive substrate; Z_w is the electron transport resistance within TiO_2 film (in Table 1 denoted by R_w); R_{ct} is the charge-transfer resistance at the TiO_2/electrolyte interface, which is shunt-wound with a chemical capacitance (C_μ);[20,21] R_{SI} is the electrolyte resistance; and R_{CE} is the charge-transfer resistance at the electrolyte/Pt counter-electrode interface. The electron lifetime (τ_n) can be drawn by the positions of the low frequency peak in Figure 2b through $\tau_n = 1/2\pi f$ (f means the frequency of superimposed ac voltage).[20] The effective diffusion coefficient (D_{eff}) and diffusion length (L_n) of electron are calculated according to the following equations:[2,22]

$$D_{eff} = (R_k/R_w)(L_F^2/\tau_n) \quad (2)$$

$$L_n = (\tau_n D_{eff})^{1/2} \quad (3)$$

where L_F is the film thickness, and R_k is the electron recombination resistance. The fitted electron transport/recombination parameters are shown in Table 1, in which R_s includes R_{FTO} and R_{SI}.

The effects of Mg^{2+} concentrations on the electron transport/recombination parameters can be explained as follows: R_s values for the modified TiO_2 electrodes are shown in all cases to increase with different extents as compared to the unmodified one as shown in Table 1. After Mg^{2+}-modifications, the MgO

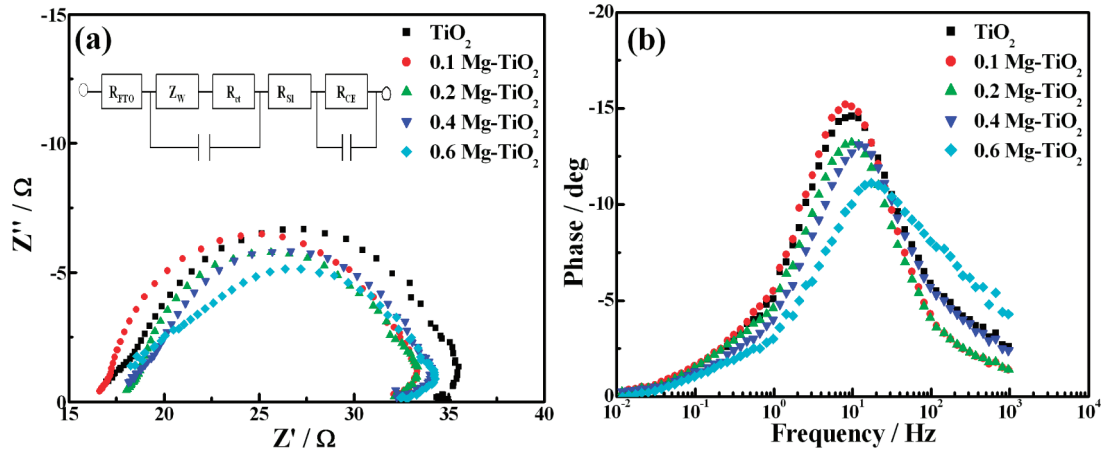

Figure 2. EIS spectra of DSSCs made with m-TiO_2 electrode and its modified products derived from different Mg^{2+} concentrations; film thickness is ca. 4.45 μm. (a) Nyquist plots; (b) Bode phase plots.

dispersed on the electrode surfaces can decrease the electric contact area at the TiO_2/electrolyte interfaces, and result in the increase of R_s values. Moreover, the MgO overlayer can also passivate the surface states of TiO_2 electrode, which is similar to the situation for the passivation of Al_2O_3 to the TiO_2 surface states in the TiO_2/Al_2O_3 core−shell structures.[8] At this point, the contribution resulting from the charge recombination due to the TiO_2 conduction band (CB) electron states becomes gradually notable,[8,17] and it is sufficient to compensate the losses in the reduced contact area with the electrolyte due to the MgO overlayer. Therefore, the modified electrodes show smaller R_{ct} values as compared to the unmodified one. The R_w values show first slightly decreasing and then increasing trends upon enhancing the Mg^{2+} concentration. On the one hand, the decrease in mean grain sizes after the modification can lead to more efficient electron transport within TiO_2 film, and then the decreased R_w value. On the other hand, the amounts of MgO immingled among TiO_2 network due to the part reconstruction of porous film are gradually increased upon enhancing the Mg^{2+} concentration, which can retard the electron transport, and result in the increased R_w value. Moreover, the L_n and D_{eff} values show no significant change under low Mg^{2+} concentrations and are significantly decreased upon further enhancing the Mg^{2+} concentration as shown in Table 1.

As can be seen from Figure 2b, only one frequency peak can be obviously observed and attributable for the electron accumulation/transport within TiO_2 film and the charge-transfer at the TiO_2/electrolyte interfaces. The frequency peak related to the I_3^- diffusion is not observed due to the low viscosity of the present electrolyte.[17] Electron lifetimes (τ_n) for all modified electrodes show a decreasing trend as a whole except for the 0.1 Mg−TiO_2 electrode with a prolonged electron lifetime. The Mg^{2+} concentration would influence the bulk traps (the localized electronic states within the bandgap of TiO_2) and surface states (the electron states physically located either at the surface of nanoparticles or within its tunneling distance) in the TiO_2 films,[7] which further lead to changes in the electron transport and recombination processes for the operation of DSSCs. For example, if the bulk trap density in film is high, the τ_n value should be large.[17] Therefore, the above shortened lifetimes indicate the decreased amount of bulk traps in TiO_2 film after the modifications.[17,20] Nevertheless, the τ_n values in all cases tested are enough for the electron injection and transport because the decay rate of N719 dye in an excited state is observed on a nanosecond time scale.[17,23]

The above variation trends in the electron transport/recombination parameters can be ascribed to different existing states of MgO. MgO overlayer, as barrier layers, can suppress the surface states of the TiO_2 electrode, which is beneficial for retarding the interfacial charge recombination, and then result in the decreased R_{ct} values. On the other hand, some MgO immingled among TiO_2 network can retard the electron transport within electrodes, and result in the increased R_w and the decreased D_{eff} and L_n values. The difficult electron transports in the modified films would result in more chances for the charge recombination. The R_{ct} for all cells tested, however, is larger than the corresponding R_w as shown in Table 1, indicating the injected electrons can smoothly transport to the conductive substrate, resulting in preferable electron collecting efficiency regardless of the relatively difficult electron transports.

3.3. Open-Circuit Voltage Decay (OCVD) Curves of Mg^{2+}-Modified Electrodes. OCVD curves can show the main information of the recombination process between the injected electrons in TiO_2 electrode and electrolyte, and the transport

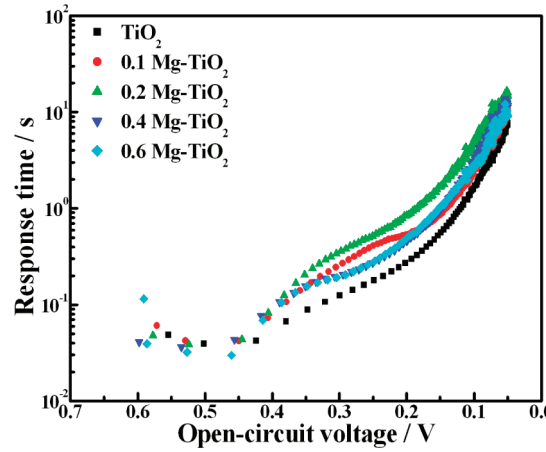

Figure 3. $\tau_n'-V_{oc}$ curves of DSSCs made with m-TiO_2 electrode and its modified products derived from different Mg^{2+} concentrations.

resistance in the film does not affect the measurements because no current is flowing through the cell under the open-circuit and dark state.[6,17−20] The recombination response time (τ_n') is given by the reciprocal of derivative of the decay curve normalized by the thermal voltage as eq 4.[6,20,24]

$$\tau'_n = \frac{k_B T}{e}\left(\frac{dV_{oc}}{dt}\right)^{-1} \quad (4)$$

where k_B is the Boltzmann coefficient, T is the temperature, and e is the elementary charge.

Figure 3 shows the effects of Mg^{2+} concentration on the τ_n' value of TiO_2 electrodes. According to Bisquert's viewpoint,[18] the $\tau_n'-V_{oc}$ curves can be marked off as three voltage-dependent regions: (1) a constant lifetime at high V_{oc} region mainly dominated by the electron transfer process from the CB of TiO_2 to the electrolyte; (2) an exponential increase region due to the internal trapping and/or detrapping; and (3) an inverted parabola at low V_{oc} region coming from the effect of surface states.

In high V_{oc} region, the $\tau_n'-V_{oc}$ curves for DSSCs made with 0.1 Mg−TiO_2 and 0.6 Mg−TiO_2 film show downward trends, indicating the recombination reactions are mainly influenced by the surface states.[17,22] As for the 0.1 Mg−TiO_2 electrode, the straight line in the $\tau_n'-V_{oc}$ curve (Figure 3) is obviously broader than the other modified electrodes, indicating more bulk traps in this electrode. This is consistent with its prolonged electron lifetime (19.72 ms, Table 1). The above phenomena can be ascribed to the MgO dispersed among TiO_2 network, which acted as bulk traps, whereas the MgO covered on film surfaces can passiviate the surface states and can contribute simultaneously a few surface states. Therefore, $\tau_n'-V_{oc}$ curves for the modified cells show an upward shift as a whole at low V_{oc} region, and a downward shift at high V_{oc} region as compared to the unmodified one. Similarly, electrons in low V_{oc} regions for all modified cells tested show longer recombination reaction times, indicating that the modified films contain fewer surface states. Among those, the 0.2 Mg−TiO_2 electrode shows the longest recombination reaction times at low V_{oc} region, indicating that the MgO modification at present situation can preferably passivate the surface states of TiO_2 film.

Upon enhancing the Mg^{2+} concentration to 0.4 M, some surface states would reappear because the MgO on the TiO_2 surfaces congregated, and then the inversed parabola in the $\tau_n'-V_{oc}$ curve at low V_{oc} region shows a downward shift. Further enhancing the Mg^{2+} concentration to 0.6 M, the straight line

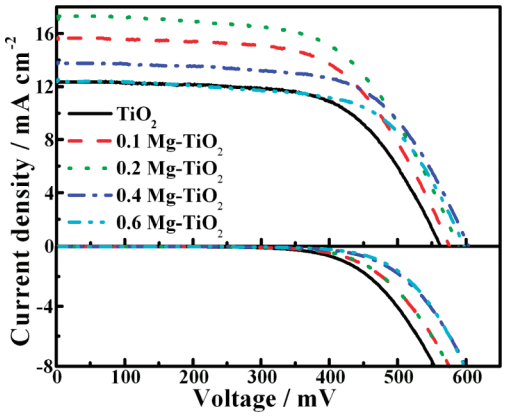

Figure 4. $I-V$ curves of DSSCs made with m-TiO_2 electrode and its modified products derived from different Mg^{2+} concentrations under 100 mW cm^{-2} light irradiation and in the dark (bottom portion, scan rate is 10 mV s^{-1}).

TABLE 2: Effects of Mg^{2+}-Modification on the Photoelectrochemical Parameters of DSSCs Fabricated with Various m-TiO_2 Electrodes

electrodes	TiO_2	0.1 Mg−TiO_2	0.2 Mg−TiO_2	0.4 Mg−TiO_2	0.6 Mg−TiO_2
η (%)	4.38	5.49	6.07	5.27	4.71
FF	0.63	0.61	0.60	0.63	0.63
I_{sc} (mA cm^{-2})	12.4	15.6	17.3	13.8	12.5
V_{oc} (mV)	562	575	588	604	598
adsorbed dye ($\times 10^{-7}$ mol cm^{-2})	0.23	0.32	0.36	0.41	0.45

and inversed parabola in the $\tau_n'-V_{oc}$ curve remain basically unchanged, indicating the distributing states for the bulk traps and the surface states resulting from TiO_2 film itself have already stabilized. Generally, excessive surface states lead to quicker electron recombination, while more bulk traps can prolong the electron lifetime, which will enhance the charge recombination probability. If the above two factors can maintain certain balance, it would decrease the electron losses due to the charge recombination and improve the cell performance. Therefore, it could be concluded that the effects of both surface states and bulk traps on the charge recombination are least for the 0.2 Mg−TiO_2 electrode; it is the reason that the corresponding solar cell shows the highest efficiency among all cells tested as shown in the following section.[17]

3.4. Photovoltaic Performances of Mg^{2+}-Modified DSSCs. $I-V$ curves of DSSCs made with different electrodes are plotted in Figure 4, and the corresponding operation parameters are summarized in Table 2. As can be seen, the efficiency (η), I_{sc}, and V_{oc} for the modified cells are enhanced with different extents. The solar cell achieving with 0.2 Mg−TiO_2 electrode shows the optimal efficiency, resulting in 39% improvement of efficiency as compared to the unmodified one, which is consistent with previous literature.[8−11,25,26]

The kinetics of recombination process is considered as one of the most important factors that control the photovoltaic performance of solar cells.[11] As can be seen from Table 2, all Mg^{2+}-modified solar cells show much higher V_{oc} than does the unmodified one. MgO covered on electrode surface, as an energy barrier, could slow the recombination rate and reduce the dark current contributed by the recombination, and then bring about a higher V_{oc}.[4,7−11] The 0.4 Mg−TiO_2 and 0.6 Mg−TiO_2 electrodes show much lower dark currents than the others, whereas the unmodified cell gives the largest one as shown in Figure 4. This changing trend in the dark current contributed to the different V_{oc} values as shown in Table 2. However, the largest V_{oc} appeared at the 0.4 Mg−TiO_2 electrode but not the 0.6 Mg−TiO_2 electrode. The possible reason might be that the retardation of recombination reactions is dependent upon the existing states of MgO, and excessive modification results in more MgO immingled among the TiO_2 network, and then more difficult electron transport due to its insulatibity. This can be validated from the largest R_w for the 0.6 Mg−TiO_2 electrode (Table 1).

In addition to the retarded recombination as energy barrier, however, the MgO overlayer has another potential advantage to improve the efficiency. As can be seen from Table 2, the dye adsorbed capacity on TiO_2 electrode gradually increased upon enhancing the Mg^{2+} concentration. The carboxyl groups in dye molecule (N719) are more easily adsorbed to the MgO overlayer because MgO with PZC of 12.0 is supposed to be the highest basic oxide.[9−11] The above increased adsorbed capacity is beneficial for enhancing the light utilization efficiency and the photogenerated carrier formation rate, and leading to the improved V_{oc}, I_{sc}, and efficiency of solar cell.[7−11] However, the optimal I_{sc} was obtained at 0.2 Mg−TiO_2 but not at 0.6 Mg−TiO_2 electrode, although its adsorbed capacity is the highest one. As can be seen from Table 1, the 0.2 Mg−TiO_2 electrode shows relatively smaller R_{ct} and R_w values, indicating the limited effects of the surface states at this electrode, and the photogenerated electrons can inject efficiently into the CB of TiO_2. Moreover, the limited effect of bulk traps on the electron transport in this film as mentioned above also contributes to the largest I_{sc}. Upon enhancing the Mg^{2+} concentration to 0.4 and 0.6 M, excessive MgO among TiO_2 network leads to more difficult electron transport, and therefore the I_{sc} values for the solar cells fabricated with these electrodes are decreased. Moreover, excessive MgO covered on electrode may suppress the electron injection by tunneling.[6,9]

On the basis of the above discussions, the porous structures of film and mesoporous structures within m-TiO_2 nanoparticles can partly collapse and reconstruct during the second annealing process, and result in some MgO immingled among TiO_2 network and covered on electrode surfaces. Generally, the present modification leads to the simultaneous increase in V_{oc} and I_{sc}, and then to improvements in efficiency with different extents, although those existing states of MgO show different influences on the photoelectrochemical characteristics of the solar cell. Therefore, it could be thought that MgO has reasonable CB levels and existing states in the present processes, which can both suppress the charge recombination efficiently and allow the electron injection to the CB of TiO_2. Moreover, the negative shift of flat-band (FB) potentials of TiO_2 nanoparticles due to the MgO overlayers results in an increase in the driving forces of electron injection, and then in the improved performance of solar cell.[8−11] The above investigation indicates that controlling the extrinsic parameters such as the electron transport and recombination by using Mg^{2+} modification is promising for improving the efficiency of TiO_2-based solar cell.

4. Conclusions

The effects of Mg^{2+} modification on the electron transport and recombination characteristics of porous electrodes derived from mesoporous TiO_2 nanoparticles were studied under applied bias by photoelectrochemical techniques. The experimental results indicate that the present Mg^{2+} modification can have two adverse effects dependent on its existing states. The MgO overlayers on TiO_2 electrode surfaces can restrain the surface states of TiO_2 electrode, and result in the decreased interfacial

charge-transfer and solution resistances, whereas some MgO immingled among TiO_2 network can retard the electron transport within electrodes, and result in the increased electron transport resistances and the decreased efficient diffusion coefficient and lengths. The optimal conversion efficiency is obtained from solar cell fabricated by TiO_2 electrode modified with 0.2 M Mg^{2+} solution, with a 39% improvement in the efficiency as compared to the unmodified one. The effects of both surface states and bulk traps on the charge recombination are least for the 0.2 $Mg-TiO_2$ electrode, which leads to increases in both the short-circuit photocurrent density and the open-circuit photovoltage, and to an obvious improvement of overall conversion efficiency, indicating the promising application in the TiO_2-based solar cells of the present Mg^{2+} modification.

Acknowledgment. This work was supported by the Natural Science Foundation of China (20871096, 20973128), the Program for New Century Excellent Talents in University (NCET-07-0637), and the Fundamental Research Funds for the Central Universities (2081003) of China.

References and Notes

(1) O'Regan, B.; Grätzel, M. *Nature* **1991**, *353*, 737.

(2) Wang, Q.; Moser, J. E.; Grätzel, M. *J. Phys. Chem. B* **2005**, *109*, 14945.

(3) Nazeeruddin, M. K.; Kay, A.; Rodicio, I.; Humphry-Baker, R.; Muller, E.; Liska, P.; Valchopoulos, N.; Grätzel, M. *J. Am. Chem. Soc.* **1993**, *115*, 6382.

(4) Kim, K. E.; Jang, S. R.; Park, J.; Vittal, R.; Kim, K. J. *Sol. Energy Mater. Sol. Cells* **2007**, *91*, 366.

(5) Zaban, A.; Chen, S. G.; Chappela, S.; Gregg, B. A. *Chem. Commun.* **2000**, 2231.

(6) Cheng, P.; Deng, C. S.; Dai, X. M.; Li, B.; Liu, D. N.; Xu, J. N. *J. Photochem. Photobiol., A* **2008**, *195*, 144.

(7) Yang, S. M.; Huang, Y. Y.; Huang, C. H.; Zhao, X. S. *Chem. Mater.* **2002**, *14*, 1500.

(8) Zhang, X. T.; Liu, H. W.; Taguchia, T.; Meng, Q. B.; Satoa, O.; Fujishima, A. *Sol. Energy Mater. Sol. Cells* **2004**, *81*, 197.

(9) Palomares, E.; Clifford, J. N.; Haque, S. A.; Lutz, T.; Durrant, J. R. *J. Am. Chem. Soc.* **2003**, *125*, 475.

(10) Jung, H. S.; Lee, J. K.; Nastasi, M. *Langmuir* **2005**, *21*, 10332.

(11) Bandara, J.; Pradeep, U. W. *Thin Solid Films* **2008**, *517*, 952.

(12) Kumara, G. R. A.; Okuya, M.; Murakami, K.; Kaneko, S.; Jayaweera, V. V.; Tennakone, K. *J. Photochem. Photobiol., A* **2004**, *164*, 183.

(13) Taguchi, T.; Zhang, X. T.; Sutanto, I.; Tokuhiro, K.; Rao, T. N.; Watanabe, H.; Nakamori, T.; Uragami, M.; Fujishima, A. *Chem. Commun.* **2003**, 2480.

(14) Grinis, L.; Kotlyar, S.; Rühle, S.; Grinblat, J.; Zaban, A. *Adv. Funct. Mater.* **2010**, *20*, 282.

(15) Peng, T. Y.; Zhao, D.; Dai, K.; Shi, W.; Hirao, K. *J. Phys. Chem. B* **2005**, *109*, 4947.

(16) Peng, T. Y.; Zhao, D.; Song, H. B.; Yan, C. H. *J. Mol. Catal. A: Chem.* **2005**, *238*, 119.

(17) Zhao, D.; Peng, T. Y.; Lu, L. L.; Cai, P.; Bain, Z. Q. *J. Phys. Chem. C* **2008**, *112*, 8486.

(18) Bisquert, J.; Zaban, A.; Greenshtein, M.; Mora-Seró, L. *J. Am. Chem. Soc.* **2004**, *126*, 13550.

(19) Wang, Z. S.; Kawauchi, H.; Kashima, T.; Arakawa, H. *Coord. Chem. Rev.* **2004**, *248*, 1381.

(20) Kern, R.; Sastrawan, R.; Ferber, J.; Stangl, R.; Luther, J. *Electrochim. Acta* **2002**, *47*, 4213.

(21) Fabregat-Santiago, F.; Garcia-Cañadas, J.; Palomares, E.; Clifford, J. N.; Haque, S. A.; Durrant, J. R.; Garcia- Beimonte, G.; Bisquert, J. *J. Appl. Phys.* **2004**, *96*, 6903.

(22) Wu, J. J.; Chen, G. R.; Yang, H. H.; Ku, C. H.; Lai, J. Y. *Appl. Phys. Lett.* **2007**, *90*, 213109.

(23) Hoshikawa, T.; Yamada, M.; Kikuchi, R.; Eguchi, K. *J. Electrochem. Soc.* **2005**, *152*, E68.

(24) Zaban, A.; Greenshtein, M.; Bisquert, J. *ChemPhysChem* **2003**, *4*, 859.

(25) Diamant, Y.; Chen, G. G.; Melamed, O.; Zaban, A. *J. Phys. Chem. B* **2003**, *107*, 1977.

(26) Lee, S.; Kim, J. Y.; Youn, S. H.; Park, M.; Hong, K. S.; Jung, H. S.; Lee, J. K.; Shin, H. *Langmuir* **2007**, *23*, 11907.

JP108446N